CLEO CONF 96-20
ICHEP96 PA05-070

Measurement of $B \to D^*\pi$ via Partial Reconstruction

CLEO Collaboration

(July 22, 1996)

Abstract

The unique kinematics of $B\overline{B}$ production at the Υ(4S) allow full reconstruction of the decay sequence $B \to D^*\pi$, $D^* \to D\pi$ without reconstruction of the D. Using $2.4 fb^{-1}$ accumulated at the Υ(4S) by the CLEO-II detector, we report measurements of $\mathcal{B}(\overline{B}^0 \to D^{*+}\pi^-) = (2.73 \pm 0.13 \pm 0.20 \pm 0.05) \times 10^{-3}$ and $\mathcal{B}(B^- \to D^{*0}\pi^-) = (4.81 \pm 0.42 \pm 0.40 \pm 0.21) \times 10^{-3}$

A. Freyberger,[1] R. Godang,[1] D. Gibaut,[1] K. Kinoshita,[1] I. C. Lai,[1] P. Pomianowski,[1] S. Schrenk,[1] G. Bonvicini,[2] D. Cinabro,[2] L. Perera,[2] B. Barish,[3] M. Chadha,[3] S. Chan,[3] G. Eigen,[3] J. S. Miller,[3] C. O'Grady,[3] M. Schmidtler,[3] J. Urheim,[3] A. J. Weinstein,[3] F. Würthwein,[3] D. M. Asner,[4] D. W. Bliss,[4] W. S. Brower,[4] G. Masek,[4] H. P. Paar,[4] J. Gronberg,[5] C. M. Korte,[5] D. J. Lange,[5] R. Kutschke,[5] S. Menary,[5] R. J. Morrison,[5] S. Nakanishi,[5] H. N. Nelson,[5] T. K. Nelson,[5] C. Qiao,[5] J. D. Richman,[5] D. Roberts,[5] A. Ryd,[5] H. Tajima,[5] M. S. Witherell,[5] R. Balest,[6] B. H. Behrens,[6] K. Cho,[6] W. T. Ford,[6] H. Park,[6] P. Rankin,[6] J. Roy,[6] J. G. Smith,[6] J. P. Alexander,[7] C. Bebek,[7] B. E. Berger,[7] K. Berkelman,[7] K. Bloom,[7] D. G. Cassel,[7] H. A. Cho,[7] D. M. Coffman,[7] D. S. Crowcroft,[7] M. Dickson,[7] P. S. Drell,[7] R. Ehrlich,[7] R. Elia,[7] A. D. Foland,[7] P. Gaidarev,[7] B. Gittelman,[7] S. W. Gray,[7] D. L. Hartill,[7] B. K. Heltsley,[7] P. I. Hopman,[7] S. L. Jones,[7] J. Kandaswamy,[7] N. Katayama,[7] P. C. Kim,[7] D. L. Kreinick,[7] T. Lee,[7] Y. Liu,[7] G. S. Ludwig,[7] J. Masui,[7] J. Mevissen,[7] N. B. Mistry,[7] C. R. Ng,[7] E. Nordberg,[7] M. Ogg,[7,*] J. R. Patterson,[7] D. Peterson,[7] D. Riley,[7] A. Soffer,[7] C. Ward,[7] P. Avery,[8] M. Athanas,[8] C. D. Jones,[8] M. Lohner,[8] C. Prescott,[8] S. Yang,[8] J. Yelton,[8] J. Zheng,[8] G. Brandenburg,[9] R. A. Briere,[9] D. Y.-J. Kim,[9] T. Liu,[9] M. Saulnier,[9] R. Wilson,[9] H. Yamamoto,[9] T. E. Browder,[10] F. Li,[10] Y. Li,[10] J. L. Rodriguez,[10] T. Bergfeld,[11] B. I. Eisenstein,[11] J. Ernst,[11] G. E. Gladding,[11] G. D. Gollin,[11] E. Johnson,[11] I. Karliner,[11] M. Palmer,[11] M. Selen,[11] J. J. Thaler,[11] K. W. Edwards,[12] A. Bellerive,[13] D. I. Britton,[13] R. Janicek,[13] D. B. MacFarlane,[13] K. W. McLean,[13] P. M. Patel,[13] A. J. Sadoff,[14] R. Ammar,[15] P. Baringer,[15] A. Bean,[15] D. Besson,[15] D. Coppage,[15] C. Darling,[15] R. Davis,[15] N. Hancock,[15] S. Kotov,[15] I. Kravchenko,[15] N. Kwak,[15] S. Anderson,[16] Y. Kubota,[16] M. Lattery,[16] J. J. O'Neill,[16] S. Patton,[16] R. Poling,[16] T. Riehle,[16] A. Smith,[16] V. Savinov,[16] M. S. Alam,[17] S. B. Athar,[17] Z. Ling,[17] A. H. Mahmood,[17] H. Severini,[17] S. Timm,[17] F. Wappler,[17] A. Anastassov,[18] S. Blinov,[18,†] J. E. Duboscq,[18] R. Fulton,[18] D. Fujino,[18] K. K. Gan,[18] T. Hart,[18] K. Honscheid,[18] H. Kagan,[18] R. Kass,[18] J. Lee,[18] M. Sung,[18] A. Undrus,[18,†] R. Wanke,[18] A. Wolf,[18] M. M. Zoeller,[18] B. Nemati,[19] S. J. Richichi,[19] W. R. Ross,[19] P. Skubic,[19] M. Wood,[19] M. Bishai,[20] J. Fast,[20] E. Gerndt,[20] J. W. Hinson,[20] D. H. Miller,[20] E. I. Shibata,[20] I. P. J. Shipsey,[20] M. Yurko,[20] L. Gibbons,[21] S. D. Johnson,[21] Y. Kwon,[21] S. Roberts,[21] E. H. Thorndike,[21] C. P. Jessop,[22] K. Lingel,[22] H. Marsiske,[22] M. L. Perl,[22] S. F. Schaffner,[22] D. Ugolini,[22] R. Wang,[22] X. Zhou,[22] T. E. Coan,[23] V. Fadeyev,[23] I. Korolkov,[23] Y. Maravin,[23] I. Narsky,[23] V. Shelkov,[23] R. Stroynowski,[23] J. Staeck,[23] I. Volobouev,[23] J. Ye,[23] M. Artuso,[24] A. Efimov,[24] M. Gao,[24] M. Goldberg,[24] R. Greene,[24] F. Frasconi,[24] D. He,[24] S. Kopp,[24] G. C. Moneti,[24] R. Mountain,[24] Y. Mukhin,[24] S. Schuh,[24] T. Skwarnicki,[24] S. Stone,[24] X. Xing,[24] J. Bartelt,[25] S. E. Csorna,[25] V. Jain,[25] and S. Marka[25]

[1]Virginia Polytechnic Institute and State University, Blacksburg, Virginia 24061
[2]Wayne State University, Detroit, Michigan 48202
[3]California Institute of Technology, Pasadena, California 91125

---

[*]Permanent address: University of Texas at Austin.

[†]Permanent address: BINP, RU-630090 Novosibirsk, Russia.

[4]University of California, San Diego, La Jolla, California 92093
[5]University of California, Santa Barbara, California 93106
[6]University of Colorado, Boulder, Colorado 80309-0390
[7]Cornell University, Ithaca, New York 14853
[8]University of Florida, Gainesville, Florida 32611
[9]Harvard University, Cambridge, Massachusetts 02138
[10]University of Hawaii at Manoa, Honolulu, Hawaii 96822
[11]University of Illinois, Champaign-Urbana, Illinois 61801
[12]Carleton University, Ottawa, Ontario, Canada K1S 5B6
and the Institute of Particle Physics, Canada
[13]McGill University, Montréal, Québec, Canada H3A 2T8
and the Institute of Particle Physics, Canada
[14]Ithaca College, Ithaca, New York 14850
[15]University of Kansas, Lawrence, Kansas 66045
[16]University of Minnesota, Minneapolis, Minnesota 55455
[17]State University of New York at Albany, Albany, New York 12222
[18]Ohio State University, Columbus, Ohio 43210
[19]University of Oklahoma, Norman, Oklahoma 73019
[20]Purdue University, West Lafayette, Indiana 47907
[21]University of Rochester, Rochester, New York 14627
[22]Stanford Linear Accelerator Center, Stanford University, Stanford, California 94309
[23]Southern Methodist University, Dallas, Texas 75275
[24]Syracuse University, Syracuse, New York 13244
[25]Vanderbilt University, Nashville, Tennessee 37235

I. INTRODUCTION

Both CLEO and ARGUS have reported measurements of the decays $\overline{B}^0 \to D^{*+}\pi^-$ and $B^+ \to D^{*0}\pi^+$ [1,2] where all final state particles were reconstructed. Partial reconstruction, where the D decay products are ignored, is attractive since ignoring the D decay products increases the acceptance for $B \to D^*\pi$ events by an order of magnitude and removes all dependence on the D decay branching ratio measurements. Previous partial reconstructions [3] have used energy and momentum conservation to determine the D momentum and the angle between it and the slow pion direction. The azimuthal angle around the slow pion direction was chosen to maximize the reconstructed the B mass. In this paper we use a partial reconstruction technique [4] in which the B mass is an input to the reconstruction. This allows all of the degrees of freedom of the decay to be determined up to a quadratic ambiguity.

The decay sequence $B \to D^*\pi_\mathrm{f}$, $D^* \to D\pi_\mathrm{s}$ is reconstructed using only the two pions. The pion produced in the B decay has a momentum of more than 2.0 GeV/c and is labeled as π_f. The pion from the D* decay has a momentum between 0.1 and 0.2 GeV/c and is labeled as π_s. We categorize the decay chains by whether the D* decay produces a charged or neutral pion.

Charged pions from D* decay are produced by:

$$\begin{aligned} \overline{B}^0 &\to D^{*+}{\pi_\mathrm{f}}^- \\ &\qquad \to\ D^0{\pi_\mathrm{s}}^+ \end{aligned}$$

these are refered to as $\pi_f^-\pi_s^+$ events. Charged conjugation is implied throughout this paper.

Neutral pions from D* decay are produced by:

$$\begin{aligned} \overline{B}^0 &\to D^{*+}{\pi_\mathrm{f}}^- \\ &\qquad \to\ D^+{\pi_\mathrm{s}}^0 \\ B^- &\to D^{*0}{\pi_\mathrm{f}}^- \\ &\qquad \to\ D^0{\pi_\mathrm{s}}^0 \end{aligned}$$

these are refered to as $\pi_f^-\pi_s^0$ events.

The $\overline{B}^0$ branching fraction to $D^{*+}\pi$ will be determined from a fit to the $\pi_f^-\pi_s^+$ events. The B^- branching fraction to $D^{*0}\pi$ will be determined from the fit to $\pi_f^-\pi_s^0$ events with the $\overline{B}^0$ contribution fixed from the $\pi_f^-\pi_s^+$ fit.

II. DATA SAMPLE AND EVENT SELECTION

The data used in this analysis were selected from hadronic events produced in e^+e^- annihilations at the Cornell Electron Storage Ring (CESR). The data sample consists of $2.39 fb^{-1}$ collected by the CLEO-II detector at the $\Upsilon(4S)$resonance (referred to as 'on-resonance') and $1.13 fb^{-1}$ at a center-of-mass energy just below the threshold for production of $B\overline{B}$ pairs (referred to as 'off-resonance' or 'continuum'). The on-resonance data corresponds to 2.560×10^6 $B\overline{B}$ pairs. The off-resonance data is used to model the continuum background. Hadronic events are selected by requiring a minimum of three charged tracks, a total visible energy greater than 15% of the center-of-mass energy, and a primary vertex within ± 5 cm in the z direction and ± 5 mm in the $r-\phi$ plane from the nominal collision point.

The CLEO II detector [5] measures both charged and neutral particles with excellent resolution and efficiency. Charged particles are measured in a 1.5 Tesla magnetic field through three nested cylindrical drift chambers covering 94% of the solid angle. These chambers are followed by time-of-flight (TOF) counters. Particle identification is accomplished by combining specific ionization (dE/dx) information from the drift chambers with TOF information. The CsI calorimeter provides excellent resolution for the reconstruction of photons. Information from an electromagnetic calorimeter and muon chambers can be used to help reject electrons and muons as π candidates.

Since the B mesons are produced almost at rest, their decay products are, on average, uniformly distributed throughout the volume of the detector. This produces events that tend to be 'spherical' in shape. Continuum events are more jetlike in shape. In order to select events that are consistent with the hypothesis of $B\overline{B}$ production, we choose events that are spherical using the shape variable R_2 [6]. This variable is the ratio of the second Fox-Wolfram moment to the zeroth moment and has been found to be useful in discriminating between $B\overline{B}$ events and those producing lighter quarks. We also require that the events we use have no charged tracks with momentum greater than 2.45 GeV. This cut rejects a small fraction of continuum events without rejecting any significant amount of signal.

All candidate charged pions are required to be consistent with being produced at the primary event vertex. In addition, we use only charged tracks with $|\cos\theta| < 0.91$ with respect to the beamline, requiring that they pass through the central drift chambers described above.

Isolated photons are paired to form π^0 candidates. Combinations which lie within 2.5 standard deviations of the nominal π^0 mass are accepted as π^0 candidates. The photon momentum vectors are then kinematically constrained to the nominal π^0 mass.

We require consistency with the pion hypothesis for all π_{f} candidates by requiring that the dE/dX and TOF information are within three standard deviations of the expected values when the information is available. When not available, no cut is made.

We use information from the muon counters and the calorimeter to reduce the number of muons and electrons which can fake the π_{f}. These vetos are used only when the information from these detector elements is available and are not applied to π_{s} candidates.

III. RECONSTRUCTION METHOD

A. Variables and Constraints

As mentioned above, this technique allows full reconstruction of the decay sequence without any reconstruction of the D decay products.. Consider the decay sequence: $B \to D^*\pi_{\mathrm{f}}$, $D^* \to D\pi_{\mathrm{s}}$. There are five particles in this decay chain, $(B$,D^*,π_{f},D,$\pi_{\mathrm{s}})$. Four variables (a 4-momentum) are required to describe each particle. A total of $20 = 5\times 4$ variables are then needed to completely describe the B decay sequence.

The constraints we exploit are:

- Energy-momentum conservation in the two decays ($4\times 2 = 8$ constraints).

- The B mass (1 constraint).
- The B energy, given by the beam energy of CESR (1 constraint).
- The D* mass (1 constraint).
- The measured four momentum of the $\pi_{\rm f}$ (4 constraints).
- The measured four momentum of the $\pi_{\rm s}$ (4 constraints).
- The mass of the D (1 constraint).

This gives 20 constraints, just enough to cover the variables and produce a complete solution for the unknown D* 4-momentum. However, the solution is quadratic, meaning that, in general, the solutions are complex valued. When a non-zero imaginary part is required there is no physically acceptable solution. For most cases with a physically acceptable solution, there are two acceptable solutions.

After all mass assignments are assumed there are three non-trivial degrees of freedom in the $B \rightarrow D^*\pi_{\rm f}$, $D^* \rightarrow D\pi_{\rm s}$ decay chain. We choose the three degrees of freedom as: θ^*_B the angle of the fast pion momentum in the B rest frame, with respect to the B flight direction; $\theta^*_{D^*}$ the angle between the slow pion momentum and the negative of the B direction, both measured in the D* rest frame; and ϕ the angle between the $B \rightarrow D^*\pi$ and $D^* \rightarrow D\pi$ decay planes.

Measurement of the 4-vectors of the two particles provides three non-trivial quantities: $|P_{\pi_{\rm f}}|$ the magnitude of the fast pion momentum in the lab, $|P_{\pi_{\rm s}}|$ the magnitude of the slow pion momentum in the lab, and $\theta_{-\pi_{\rm f}\pi_{\rm s}}$ the angle between the fast and slow pion momenta in the lab.

Knowledge of $|P_{\pi_{\rm f}}|$ and $|P_{\pi_{\rm s}}|$ is all that is needed to determine $\cos\theta^*_B$ and $\cos\theta^*_{D^*}$. There is an almost linear relationship between the momenta and the cosines of the center of mass angles. The quantity $\cos\theta^*_B$ depends solely on $|P_{\pi_{\rm f}}|$ while $\cos\theta^*_{D^*}$ depends mainly on $|P_{\pi_{\rm s}}|$ with a small correction from $|P_{\pi_{\rm f}}|$.

Energy and momentum conservation in the B and D* decays constrain the D* direction to lie on a cone around $\vec{P}_{\pi_{\rm f}}$ and another cone around $\vec{P}_{\pi_{\rm s}}$ in the lab frame, as shown in Figure 1. The size of the cone is determined by the center of mass angle and the boost of the decaying particle. Pairs of fast and slow pions in which the two cones do not intersect have no real solution for $\vec{P}_{D^*}$ and are inconsistent with $B \rightarrow D^*\pi$ production.

The size of the opening angle around the $\pi_{\rm f}$ direction, $\theta_{-\pi_{\rm f}D^*}$ and the size of the opening angle around the $\pi_{\rm s}$ direction, $\theta_{\pi_{\rm s}D^*}$ defines a region in $\cos\theta_{-\pi_{\rm f}\pi_{\rm s}}$ space in which the fast and slow pion are consistent with $B \rightarrow D^*\pi$ production.

The center of the allowed region of $\cos\theta_{-\pi_{\rm f}\pi_{\rm s}}$, c, is given by:

$$c = \cos\theta_{-\pi_{\rm f}D^*} \times \cos\theta_{\pi_{\rm s}D^*} \tag{1}$$

and the half width of the allowed range of $\cos\theta_{-\pi_{\rm f}\pi_{\rm s}}$, w, is

$$w = \sin\theta_{-\pi_{\rm f}D^*} \times \sin\theta_{\pi_{\rm s}D^*}. \tag{2}$$

The value of the center can be subtracted from $\cos\theta_{-\pi_{\rm f}\pi_{\rm s}}$ to form a more convenient variable, s:

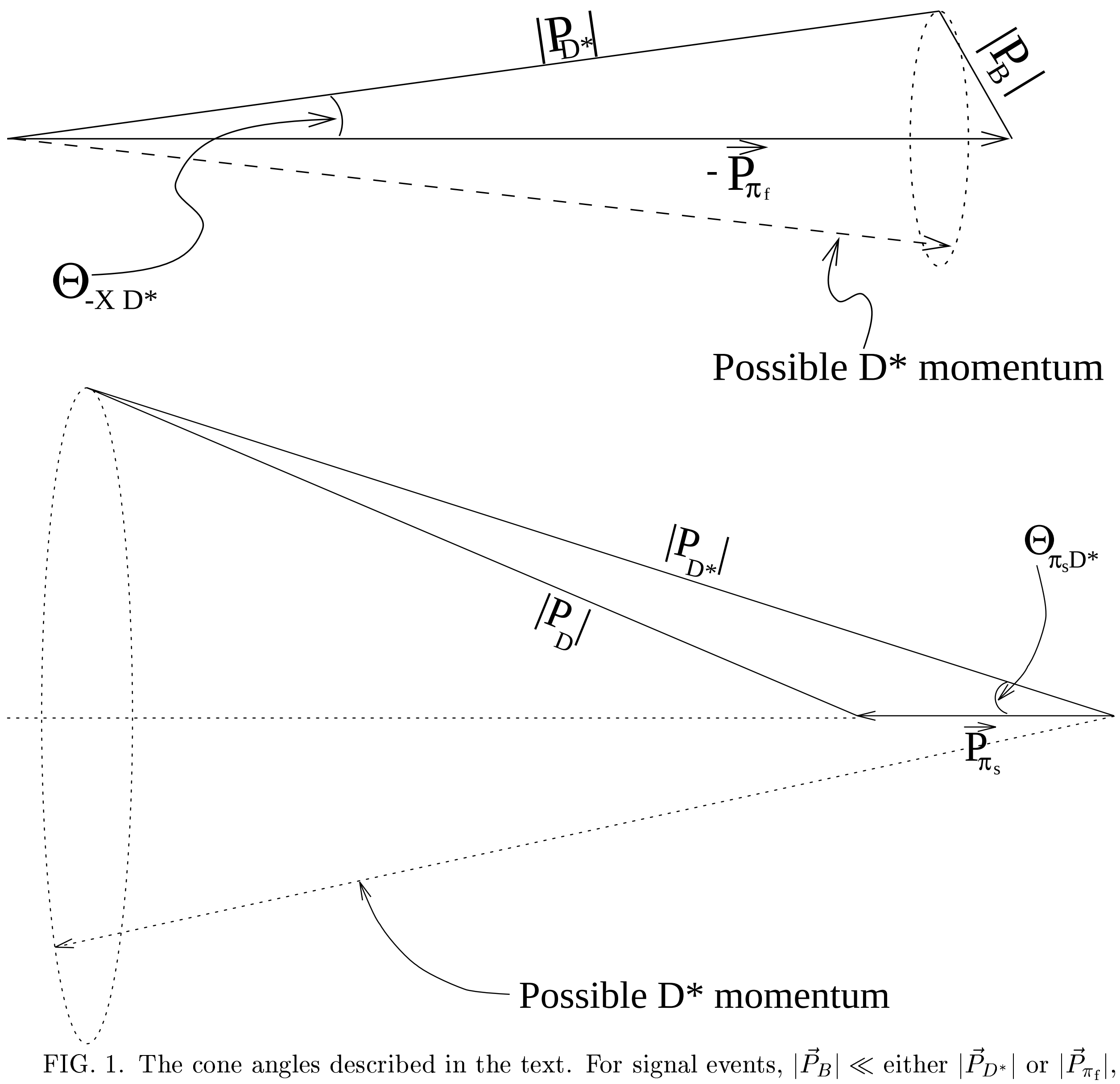

FIG. 1. The cone angles described in the text. For signal events, $|\vec{P}_B| \ll$ either $|\vec{P}_{D^*}|$ or $|\vec{P}_{\pi_\mathrm{f}}|$, and the D* must be nearly back to back with π_f.

$$s = \cos\theta_{-\pi_f\pi_s} - \cos\theta_{-\pi_f D^*} \times \cos\theta_{\pi_s D^*} \tag{3}$$

which is centered at zero for signal.

Background events and mismeasured signal events can have non-physical opening angles. When a cone angle in the lab is non-physical we set the corresponding cosine to 1 and assign $w = 0$.

Eventually, we accept only pion combinations that pass a broad cut, $|s| < w + 0.02$, designed to have a high acceptance for signal events and minimal systematic errors from smearing. A plot of s vs. w for Monte Carlo signal events is shown in Fig. 2. Monte Carlo signal events were generated by requiring one B to decay in the signal channel and allowing the other B to decay generically. The generated 4-vectors were then passed through a GEANT [7] based simulation of the CLEO-II detector.

The backgrounds tend to be flat in the variable s. However, the width of the acceptance region, w, is largest when the opening angles of the cones are physical. This variable acceptance is a large effect on the shape of the backgrounds.

B. Identification of signal

The distributions of $\cos\theta^*_{D^*}$, $\cos\theta^*_B$ are shown in Figure 3 for accepted simulated signal events, for perfect measurement and then with the simulation's measurement errors as well. Perfectly measured signal cosines should always fall between -1 and 1.

The signal distribution in $\cos\theta^*_{D^*}$ is expected to be $\propto \cos^2\theta^*_{D^*}$, because angular momentum conservation dictates that the D* be produced with zero helicity. The signal distribution in $\cos\theta^*_B$ is expected to be flat because the B is a pseudoscalar.

Smearing in these variables comes from mismeasurement of the pion momenta and from beam energy variations. Mismeasurement of the fast pion momentum dominates the Gaussian smearing in $\cos\theta^*_{D^*}$, while the tails in $\cos\theta^*_{D^*}$ arise from coulomb scattering and mismeasurement of the slow pion. Beam energy variations dominate the smearing in $\cos\theta^*_B$.

The shape of the backgrounds is primarily determined by the π_s momentum spectrum and the dependence of w on $\cos\theta^*_B$ and $\cos\theta^*_{D^*}$. This dependence causes a peaking of the background around $\cos\theta^*_{D^*}$ equal to zero. Since the signal is $\propto \cos^2\theta^*_{D^*}$ this is not a problem. Backgrounds from B decays where both pions come from the same B can have a more complicated structure.

C. Selection of two pion candidates

All candidates are required to satisfy $|s| < w + 0.02$, the back to back angle consistency cut described earlier. In addition we require $|\cos\theta^*_B| < 1.65$ and $|\cos\theta^*_{D^*}| < 5.0$. The global event shape variable, R2, is required to be less than 0.275 and 0.25 for $\pi_f^-\pi_s^+$ and $\pi_f^-\pi_s^0$ candidates, respectively. The $\pi_f^-\pi_s^+$ candidates are required to have opposite charges.

After these cuts are made there are still events in which there are multiple combinations. In the signal Monte Carlo there are 5% and 24% of events which have multiple combinations for $\pi_f^-\pi_s^+$ and $\pi_f^-\pi_s^0$ combinations, respectively. The combination with the smallest value of s is chosen for $\pi_f^-\pi_s^+$ combinations. In $\pi_f^-\pi_s^0$ combinations the candidate whose π^0 is closest to the nominal π^0 mass is chosen.

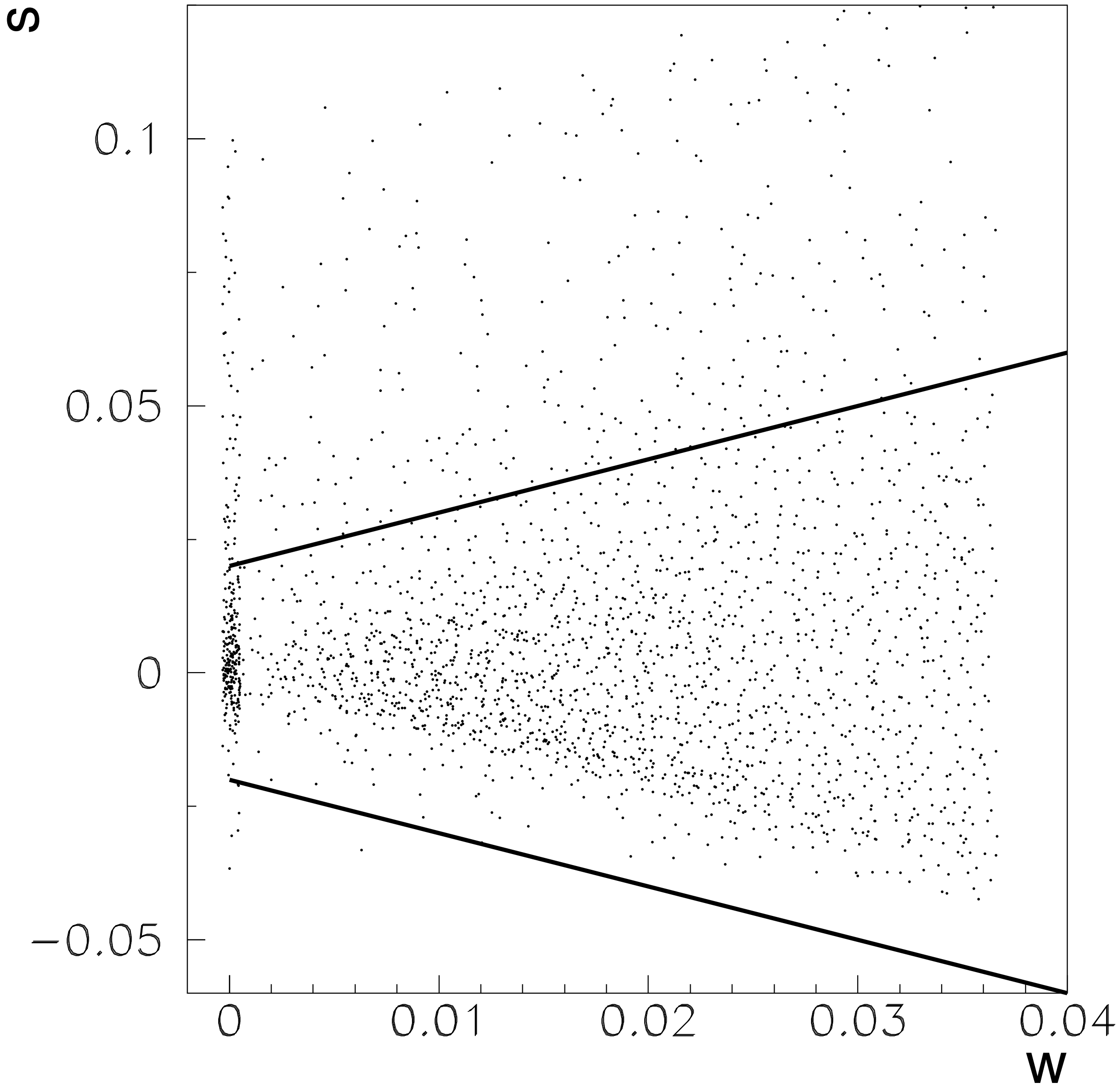

FIG. 2. Two-dimensional plot of s versus w shown for simulated signal events. The solid lines indicate the eventual acceptance region for signal. The tail outside the acceptance region is from coulomb scattering. The cluster of events at $w = 0$ are events in which mismeasurement has caused $|\cos\theta^*_B|$ or $|\cos\theta^*_{D^*}|$ to be greater than 1 and thus have a non-physical opening angle.

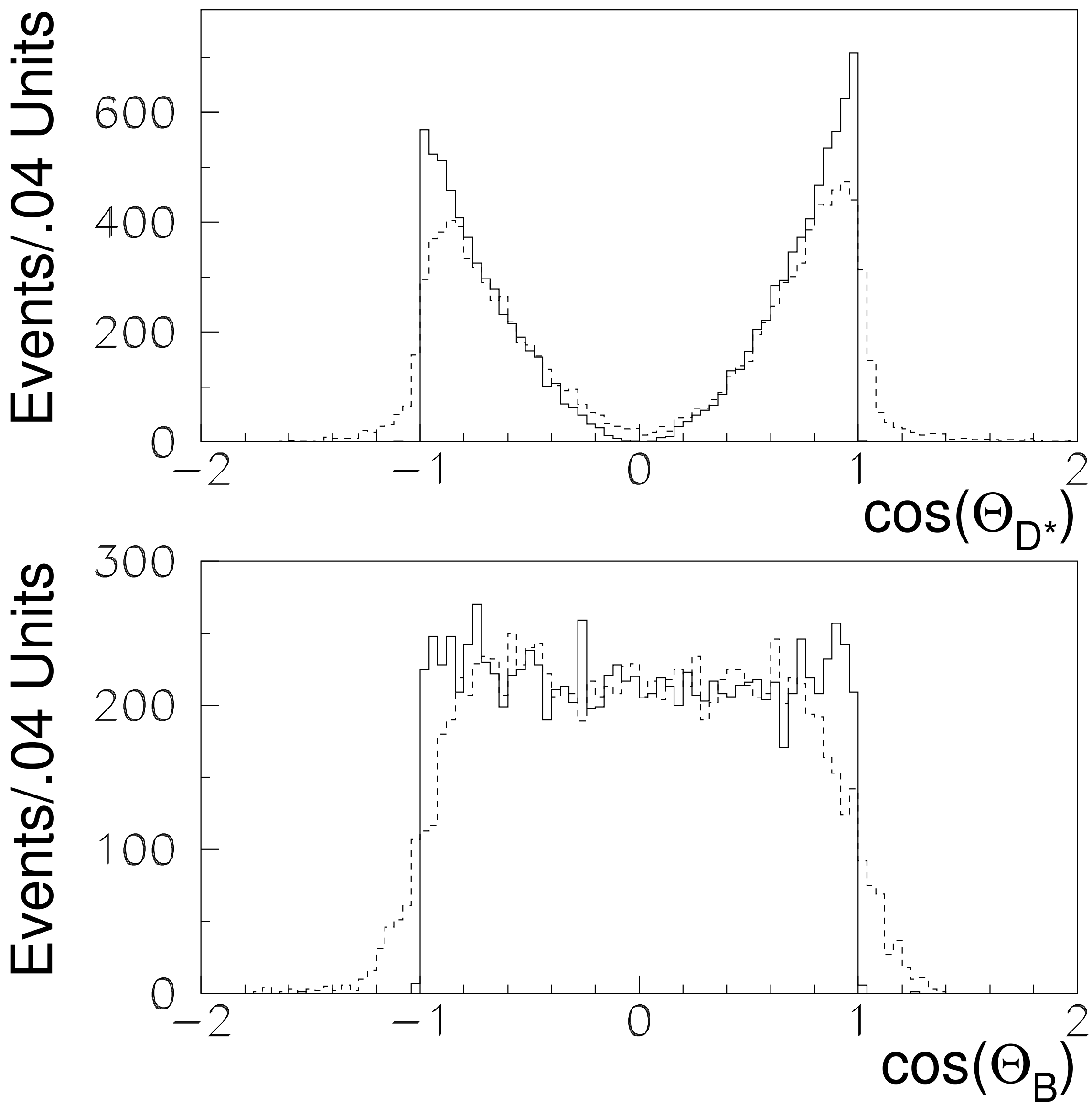

FIG. 3. Distribution of $\cos\theta^*_{D^*}$ and $\cos\theta^*_B$ for simulated signal events. The solid lines include detector acceptance but no measurement errors. The dashed is with full detector simulation.

IV. BACKGROUNDS

The dominant source of background is from continuum production of $q\overline{q}$. This background can be subtracted using a sample of data taken below the $\Upsilon(4S)$ resonance, after scaling for the relative luminosities between the on-resonant and off-resonant data.

The background from B decays is dominated by modes which decay to DX where the D can be either charged or neutral and can be in a higher spin state and where $X = \pi, \rho,$ or $\mu\nu_\mu$. The shape of the B decay background is modeled using a large sample of generic simulated $B\overline{B}$ events. We divide the total B decay background into B decay submodes which comprise a signifigant fraction of events. The submodes are listed in Table I. Submodes which are kinematically similar are combined. The branching fractions of these modes are allowed to vary in order to model the possible variation of the B decay background shape. The branching fractions of the submodes are constrained by a Gaussian to the central value and error of the world average measurement as reported in the PDG [8], or left unconstrained if no measurement is available.

The main uncertainty in the shape comes from the $B \to D^{**}\pi$ decays. Of the eight branching fractions (4 J^P states for both charged and neutral D^{**}) only one has been measured. Factorization [9], combined with the measurement of the ratio of the neutral and charged B meson production fractions [10], predicts that the branching fraction of B to neutral D^{**} is 2/3 of the branching fraction of B to charged D^{**}. This still leaves 3 decay modes unconstrained.

There are two backgrounds which scale with the signal. Their normalizations will be fixed to the signal normalization. The decay $B \to D^* K$ is nearly indistinguishable from signal. The particle identification above 2.0 GeV/c is not sufficient to separate K's from π's. The branching fraction of $B \to D^* K$ is well determined relative to $B \to D^* \pi$ by the value of the CKM matrix element $|V_{us}|$. It's contribution is small, however, and will not introduce a serious systematic error. Two pion combinations in which a real $\pi_{\rm f}$ from a $B \to D^* \pi$ decay is combined with a random $\pi_{\rm s}$ from the D decay or from the other B are called signal combinatorics. Since they contain a real $\pi_{\rm f}$ from the $B \to D^* \pi$ decay their contribution will scale with changes in the $B \to D^* \pi$ branching fraction. These events will be identical to the signal in $\cos\theta^*_B$ but will resemble background in the variable $\cos\theta^*_{D^*}$.

V. RESULTS

A. Fitting Method

To extract the branching ratios we perform a two-dimensional χ^2 fit to the data using the MINUIT [11] program. The statistical error in each bin must take into account the bin by bin subtraction of scaled off-resonant data. The error in each bin is the quadrature sum of the on-resonant error plus the off-resonant error after scaling.

The fitting function is composed of Continuum, B decay background, and signal components.

- The continuum distribution is taken from off-resonant data. It's normalization and shape are fixed in the fit.

- The B decay background distribution is taken from simulated generic $B\overline{B}$ events. The normalization is allowed to vary freely in the fit. The shape of the B decay background is dependent on the branching ratios of the different submodes. They are allowed to vary, constrained by a Gaussian to their measured central value and error from the PDG [8] when available, see Table I.

- The signal distribution is modeled by simulated $B \to D^* \pi$ events. The two backgrounds which scale with the signal, $B \to D^* K$ and signal combinatorics are also included. Figure 4 shows the projections of the signal histogram in $\cos\theta^*_{D^*}$ and $\cos\theta^*_B$ for $\pi^-_f \pi^+_s$ events. In the $\cos\theta^*_{D^*}$ histogram the left peak is smaller than the right peak due to the decreasing detector acceptance for slow charged tracks. In the $\cos\theta^*_B$ histogram the D^*K events and signal combinatorics have the same distribution as the signal. As one would expect. Figure 5 shows the same for $\pi^-_f \pi^0_s$ events. The signal combinatorics are much larger for ${\pi_s}^0$ than for ${\pi_s}^-$. However, they resemble background much more than signal and do not have a large effect on the final result. The detector acceptance is flat for π^0's.

- The fitting function for $\pi^-_f \pi^0_s$ events contains an additional component, a feedthrough of $\overline{B}^0 \to D^{*+}\pi^-$ decays where the D^{*+} decays to $D^+\pi^0$. The distribution of these events is very similar to signal. The normalization of these feedthrough events in the $\pi^-_f \pi^0_s$ fit is fixed by the value of BR($\overline{B}^0 \to D^{*+}\pi^-$) determined in the $\pi^-_f \pi^+_s$ fit.

TABLE I. The modes into which the B decay background has been subdivided. The remaining events which are not classified are allowed to vary around their prediction with a error of 25%. All other contraints are from the PDG [8]. The branching ratio for B decays to charged D^{**} is assumed to be 2/3 the branching ratio for B decays to neutral D^{**}.

Mode	Branching ratio constraint %
$B^- \to D^{*0}\pi^-$	$.52 \pm .08$
$B \to D^{+/0}\pi^-$	$.83 \pm .064$
$\overline{B}^0 \to D^{*+}\rho^-$	$.73 \pm .15$
$B^- \to D^{*0}\rho^-$	$1.55 \pm .31$
$B \to D^{+/0}\rho^-$	$2.12 \pm .23$
$\overline{B}^0 \to D^{*+}\pi^-\pi^0$	$.77 \pm .53$
$B \to D^{*+/0}\mu^-\nu_\mu$	$9.86 \pm .84$
$B \to D^{**+/0}\pi^-(2420)$	$.15 \pm .06$
$B \to D^{**+/0}\pi^-(0^+\text{wide})$	unconstrained
$B \to D^{**+/0}\pi^-(1^+\text{wide})$	unconstrained
$B \to D^{**+/0}\pi^-(2460)$	unconstrained
remaining	$1.0 \pm .25$

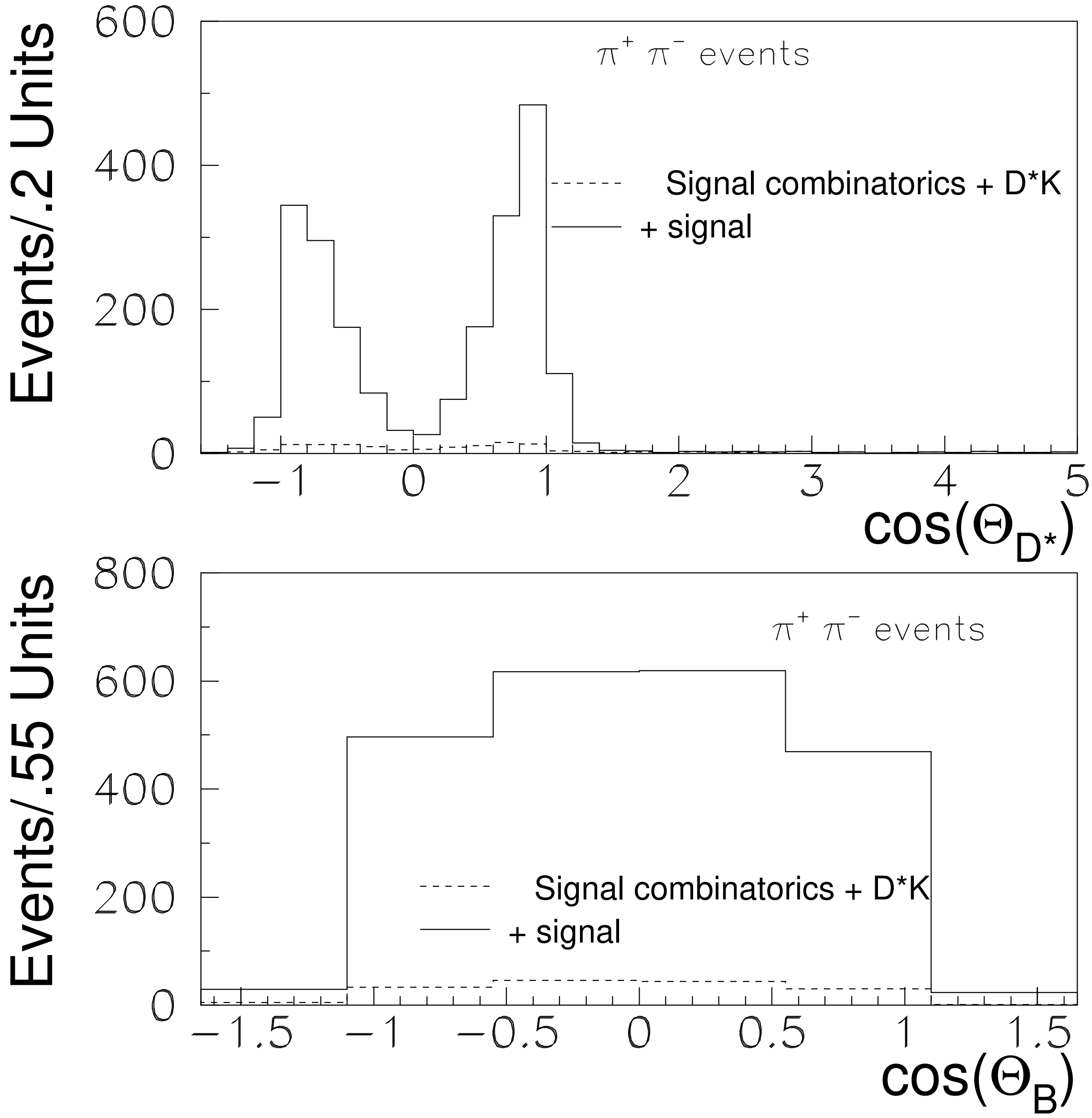

FIG. 4. The projections of the signal histogram used in the $\pi_f^- \pi_s^+$ fit.

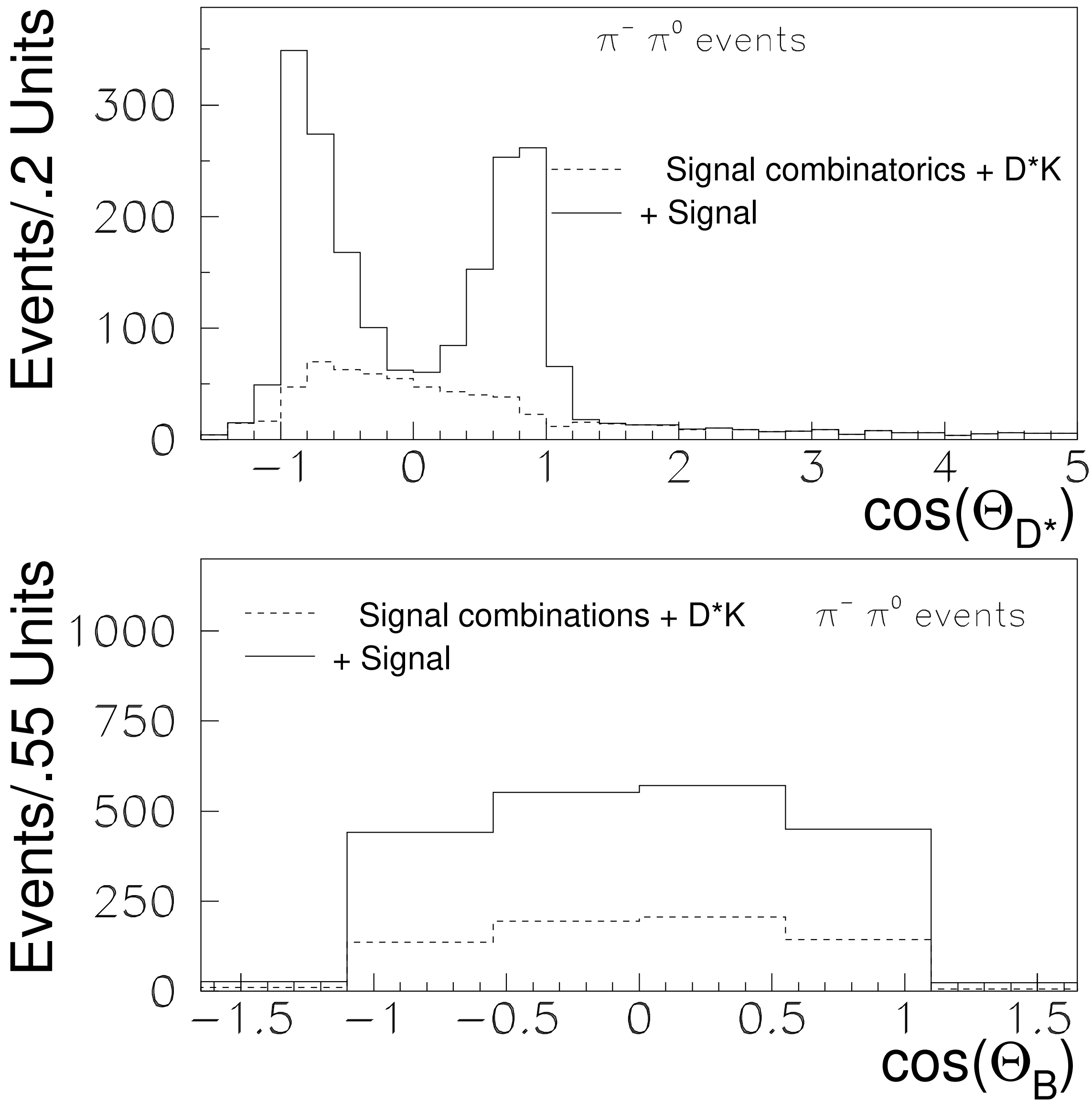

FIG. 5. The projections of the signal histogram used in the $\pi_f^- \pi_s^0$ fit.

B. Two dimensional fit results

The projections of the data and the fitting function in $\cos\theta^*_B$ and $\cos\theta^*_{D^*}$ are shown in Figure 6 for the $\pi^-_f\pi^+_s$ fit and in Figure 7 for the $\pi^-_f\pi^0_s$ fit.

The fitted number of signal events is given in Table II along with the acceptance $\times$ efficiency and the relevant D^* branching ratio. Using the value of 2.560×10^6 $B\overline{B}$ pairs produced we calculate the branching ratios to be:

$$\mathcal{B}(\overline{B}^0 \to\ D^{*+}\pi^-) = (2.73\pm0.13)\times10^{-3} \tag{4}$$

$$\mathcal{B}(B^- \to\ D^{*0}\pi^-) = (4.81\pm0.42)\times10^{-3} \tag{5}$$

TABLE II. The yield of signal events from the fits. The D* branching fractions are not included in the calculation of acceptance times efficiency.

Mode	yield	acc $\times$ eff	$\mathcal{B}(D^*\to D\pi)$
$\overline{B}^0 \to D^{*+}\pi^-; D^{*+}\to D^0\pi^+$	2050 ± 101	0.43	68.1%
$B^- \to D^{*0}\pi^-; D^{*0}\to D^0\pi^0$	1331 ± 115	0.17	63.6%

C. Systematic Errors

The systematic errors from all sources are compiled in Table III. The systematic errors from the knowledge of D* branching fractions is not included in the total.

The B decay background contains several $B\to D^{**}\pi$ modes which are unmeasured. Their branching ratios are allowed to vary freely in the fits. The fits report central values of these modes that are consistent with theoretical predictions with large correllated errors. In order to estimate the systematic error from varying all the B decay submodes we take the difference in quadrature of the error on the signal normalization with all the submodes floating and fixed. Fixing the submodes has no effect on the central value of the signal. This leads to a systematic error of 1.4% and 3.7% for the neutral and charged B branching ratios respectively.

The signal histograms contain signal combinatorics and $B\to D^*K$ events. The level of these contributions is varied by $\pm20\%$ which leads to a systematic error of 0.5% and 0.6% for the neutral and charged B branching ratios respectively.

The signal shape is smeared by track parameter mismeasurements and beam energy smearing. A parameterized signal shape whose smearing could be varied was used to fit the data. This allowed the value of the smearings to be varied by $\pm20\%$ of their central value in the Monte Carlo simulation. This leads to a systematic error of 1.3% for both branching ratios.

The cut on the event shape variable, R_2, was varied between 0.1 and 0.5. The fit was redone at each point and the variance of the result used to estimate the systematic error from

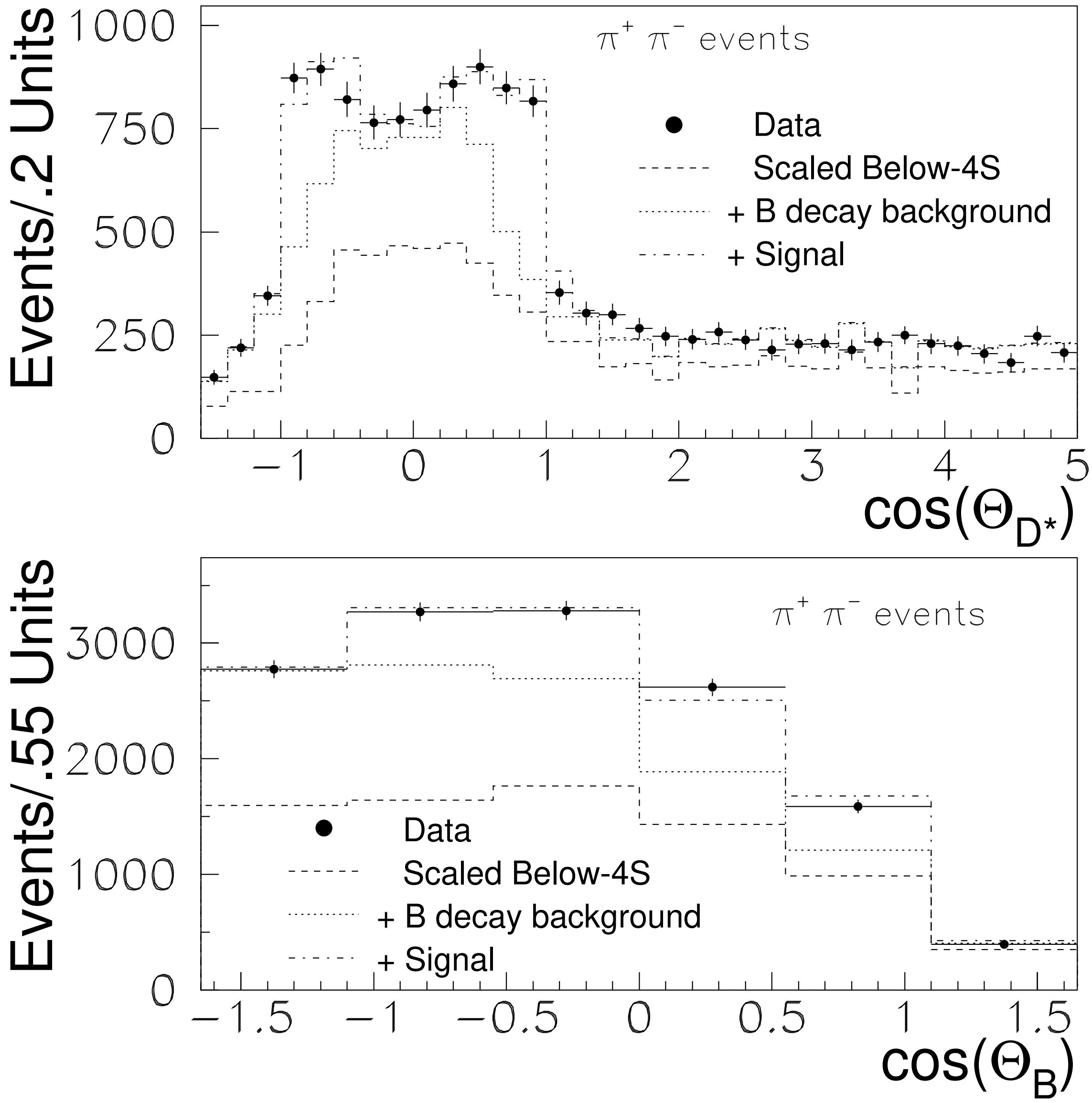

FIG. 6. The projections of the data histogram in $\cos\theta_B^*$ and $\cos\theta_{D^*}^*$ with the fitting function for the $\pi_f^-\pi_s^+$ fit.

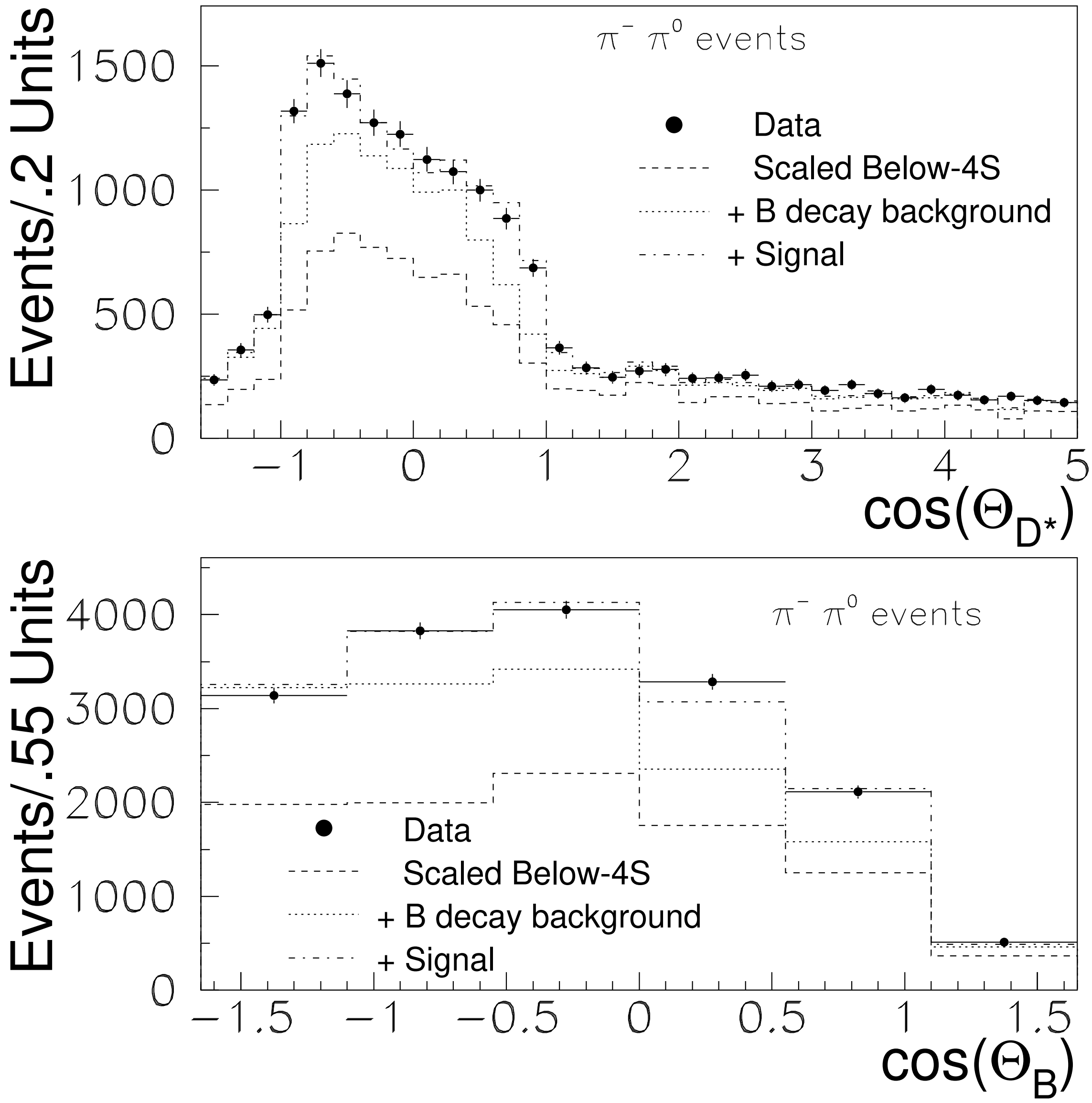

FIG. 7. The projections of the data histogram in $\cos\theta_B^*$ and $\cos\theta_{D^*}^*$ with the fitting function for the $\pi_f^-\pi_s^0$ fit.

this cut. The systematic error was 4.5% and 3.1% for the neutral and charged B branching ratios respectively.

The back to back angle consistency cut, $|s| < w + 0.02$, was varied between $|s| < w + 0.00$ to $|s| < w + 0.05$. The data was refit at each point and the variance of the result used to estimate the systematic error. The systematic error was 1.7% and 2.0% for the neutral and charged B branching ratios respectively.

The track reconstruction systematic error is 1.0% for fast charged tracks, for slow tracks it is 5.0% and 5.5% for charged and neutral pions respectively.

The feedthrough of neutral B decays into the $\pi_f^- \pi_s^0$ fit is nearly indistinguishable from signal. An increase in the number of feedthrough events decreases the number of signal events by roughly one to one. Due to the B and D* branching ratios we expect to find a ratio of signal to feedthrough events of about 4:1. By varying the feedthrough normalization we determine that $\partial\mathcal{B}(B^- \to D^{*0}\pi^-) = -0.2 \times \partial\mathcal{B}(\overline{B}^0 \to D^{*+}\pi^-)$. The total error of of 8.9% on the neutral B decay branching fraction translates into an error of 1.8% on the charged B decay branching fraction.

The simulated signal event statistics contributes a systematic error of about 1.0% and 1.3% for the neutral and charged B branching ratios respectively. The error on the charged B measurement from the neutral B feedthrough is given by 2.13% $\times 0.2$ and is thus about 0.4%.

The systematic error on the total number of $B\overline{B}$ decays 1.8%. The error comes from the uncertainty in the $\Upsilon(4S)$ cross section.

The uncertainty on the D^* branching ratios contributes a systematic error of 1.9% and 4.4% for the neutral and charged B decay branching fractions.

TABLE III. Summary of systematic errors. (%)

Systemtic	charged fit	neutral fit
B decay background shape	1.4	3.7
Signal smearing	1.3	1.3
Signal subcomponents	0.5	0.6
R2 cut	4.5	3.1
angle cut	1.7	2.0
Track reconstruction	5.0	5.5
Monte Carlo statistics	1.0	1.4
$N_{B\overline{B}}$	1.8	1.8
$D^{*+}\pi^-$ feedthrough	n/a	1.8
Total systematic	7.5	8.3
D^* branching ratios	1.9	4.4

VI. CONCLUSION

Using our estimate of the systematic error we calculate the $B \to D^* \pi$ branching fractions to be:

$$\mathcal{B}(\overline{B}^0 \to \ D^{*+}\pi^-) = (2.73 \pm 0.13 \pm 0.20 \pm 0.05) \times 10^{-3} \tag{6}$$

$$\mathcal{B}(B^- \to \ D^{*0}\pi^-) = (4.81 \pm 0.42 \pm 0.40 \pm 0.21) \times 10^{-3} \tag{7}$$

where the first error is statistical, the second is systematics, and the third comes from the uncertainty in the D^* branching ratios. The previous CLEO II measurement [1] of these modes using full reconstruction found values of:

$$\mathcal{B}(\overline{B}^0 \to \ D^{*+}\pi^-) = (2.6 \pm 0.3 \pm 0.4 \pm 0.1) \times 10^{-3} \tag{8}$$

$$\mathcal{B}(B^- \to \ D^{*0}\pi^-) = (5.2 \pm 0.7 \pm 0.6 \pm 0.4) \times 10^{-3} \tag{9}$$

The systematic errors between the two methods are largely independent. Since the partial reconstruction has an order of magnitude more events the statistical error is largely independent as well.

ACKNOWLEDGEMENTS

We gratefully acknowledge the effort of the CESR staff in providing us with excellent luminosity and running conditions. J.P.A., J.R.P., and I.P.J.S. thank the NYI program of the NSF, M.S thanks the PFF program of the NSF, G.E. thanks the Heisenberg Foundation, K.K.G., M.S., H.N.N., T.S., and H.Y. thank the OJI program of DOE, J.R.P, K.H., and M.S. thank the A.P. Sloan Foundation, and A.W., and R.W. thank the Alexander von Humboldt Stiftung for support. This work was supported by the National Science Foundation, the U.S. Department of Energy, and the Natural Sciences and Engineering Research Council of Canada.

REFERENCES

[1] CLEO Collab., M.S. Alam *et al.*, Phys. Rev. D **50** (1994) 43.
[2] ARGUS Collab., Ehrlichmann *et al.*, ZPhys. C **48** (1990) 543.
[3] CLEO Collab., R. Giles *et al.*, Phys. Rev. D **30** (1984) 2279.
[4] CLEO Collab., M. Artuso *et al.*, Phys. Lett. B **23** (1995) 1387.
[5] CLEO Collab., Y. Kubota *et al.*, Nucl. Instr. and Meth. **A320** (1992)
[6] G.C. Fox and S. Wolfram, Phys. Rev. Lett. **41** (1978) 1581.
[7] `GEANT 3.15`: R. Brun *et al.*, CERN DD/EE/84-1.
[8] L. Montanet *et al.*, Phys. Rev. D **50** (1994) 1173 and 1995 off year partial update for the 1996 edition (URL: http://pdg.lbl.gov/).
[9] J. Bjorken, Nucl. Phys. B (proc. Suppl.) **11** (1989) 325.
[10] CLEO collab., B. Barish *et al.*, Phys. Rev. D **51** (1995) 1014.
[11] I. Brock, A fitting and Plotting Package Using MINUIT, CLEO/CSN Note 245-B, Revised (1992); F. James, MINUIT, Function Minimization and Error Analysis, CERN Program Library Long Writeup D506, Mar. 1994.